Chinese Physics Letters

LETTER

Observation of Robust In-Gap Edge States in $EuRbFe_4As_4$

Cite as: Xu-Hui Ning *et al*. 2026 *Chin. Phys. Lett.* **43** 100706

DOI CSTR

Recommended Articles

Edge States and Enhanced Superconducting Gaps in Bi Islands on $FeTe_{0.55}Se_{0.45}$

Chuanhao Wen, Zhiyong Hou, Zhiyuan Shang, Huan Yang, and Hai-Hu Wen
Chin. Phys. Lett. **42**, 080707 (2025)

Hybridization Gap and Edge States in Strained-Layer InAs/$In_{0.5}Ga_{0.5}Sb$ Quantum Spin Hall Insulator

Wenfeng Zhang, Peizhe Jia, Wen-kai Lou, Xinghao Wang, Shaokui Su, Kai Chang, and Rui-Rui Du
Chin. Phys. Lett. **43**, 010704 (2026)

Floquet Non-Abelian Topological Charges and Edge States

Jiaxin Pan, and Longwen Zhou
Chin. Phys. Lett. **42**, 090706 (2025)

Enhanced Superconductivity in FeSe Thin Films on LiF Substrates

Zhiyu Huang *et al*.
Chin. Phys. Lett. **43**, 040706 (2026)

Review of the Research Status of Practical Superconducting Materials and Their Current Carrying Performance

Yifan Zhang, Shengnan Zhang, Jixing Liu, Fang Yang, Chengshan Li, Jianfeng Li, and Pingxiang Zhang
Chin. Phys. Lett. **41**, 117402 (2024)

A series journal of Chinese Physical Society distributed by IOP Publishing

Chinese Physics Letters

Chin. Phys. Lett. **43** 100706 (2026)

LETTER

DOI: 10.1088/0256-307X/43/10/100706
CSTR: 32039.14.0256-307X.43.10.100706

Observation of Robust In-Gap Edge States in $EuRbFe_4As_4$

Xu-Hui Ning(宁旭辉)[1], Sha-Sha Xue(薛莎莎)[1], Rui-Jun Xi(席瑞骏)[1], Xing-Sen Chen(陈星森)[1], Ji-Ce Sun(孙蓟策)[1], Yi Zhang(章毅)[1], Xian Du(杜宪)[1], Ting-Wen Miao(缪婷文)[1], Peng-Yu Hu(胡鹏宇)[1], Zi-Hao Ma(马子豪)[1], Shi Chen(陈石)[1], Ying-Xue Huang(黄映雪)[1], Qing-Chen Duan(段清晨)[1], Hao Yang(杨浩)[1,2,3], Dan-Dan Guan(管丹丹)[1,2,3], Wei-Jiong Chen(陈维炯)[1,2,3], He-Mian Yi(伊合绵)[1,2,3], Xiao-Xue Liu(刘晓雪)[1,2,3], Liang Liu(刘亮)[1,2,3], Yao-Yi Li(李耀义)[1,2,3], Shi-Yong Wang(王世勇)[1,2,3], Can-Hua Liu(刘灿华)[1,2,3], Hui Xing(邢晖)[1], Rui-Dan Zhong(钟瑞丹)[1], Cong-Jun Wu(吴从军)[4], Hao Zheng(郑浩)[1,2,3,*], and Jin-Feng Jia(贾金锋)[1,2,3,5,6,*]

[1]State Key Laboratory of Micro-nano Engineering Science, Tsung-Dao Lee Institute & School of Physics and Astronomy, Key Laboratory of Artificial Structures and Quantum Control (Ministry of Education), Shanghai Jiao Tong University, Shanghai 200240, China
[2]Hefei National Laboratory, Hefei 230088, China
[3]Shanghai Research Center for Quantum Sciences, Shanghai 201315, China
[4]New Cornerstone Science Laboratory, Department of Physics, School of Science, Westlake University, Hangzhou 310024, China
[5]Quantum Science Center of Guangdong-Hong Kong-Macao Greater Bay Area (Guangdong), Shenzhen 518045, China
[6]Department of Physics, Southern University of Science and Technology, Shenzhen 518055, China

*Corresponding authors. Email: haozheng1@sjtu.edu.cn; jfjia@sjtu.edu.cn

The study of in-gap excitations in a superconductor is vital for understanding its pairing symmetry and exploring Majorana boundary modes. Here, we report pronounced in-gap edge states in the iron-based superconductor $EuRbFe_4As_4$ using scanning tunneling microscopy and spectroscopy. These edge states appear at full-unit-cell and half-unit-cell steps, with a consistent spatial decay length of approximately 1.8 nm. Systematic temperature-dependent measurements show that the edge states persist above the magnetic transition temperature yet vanish upon exiting the superconducting state, linking them to superconducting pairing rather than ferromagnetism. Furthermore, the absence of interaction between adjacent edge states indicates their chiral nature. Our findings position $EuRbFe_4As_4$ as a platform for unconventional superconductivity and functional devices.

Bulk-boundary correspondence characterizes the topological properties of quantum materials. A prime example is quantum spin Hall insulators, which exhibit fully gapped bulk states and gapless helical edge states [1,2]. Scanning tunneling microscopy/spectroscopy (STM/S) observations of this gapped-to-gapless transition at edges provide direct evidence for their topological nature [3−12]. Topological superconductors have attracted interest for hosting low-energy quasiparticle excitations that satisfy Majorana equations [13,14]. Majorana zero modes have been detected via STM in various platforms, including topological insulator/superconductor heterostructures, iron-based superconductors, and magnetic atom chains on superconducting substrates [15−22]. Chiral Majorana modes appear as in-gap edge states in topological superconductors. Identifying such edge states is therefore critical [23–27].

Iron-based superconductor $EuRbFe_4As_4$ (where Eu is europium, Rb is rubidium, Fe is iron, and As is arsenic) uniquely exhibits coexistence of magnetic order and superconductivity due to localized Eu^{2+} cations. A helical antiferromagnetic order sets in well inside the superconducting state, in which the moment of Eu^{2+} orders ferromagnetically within each Eu^{2+} plane. The in-plane ferromagnetism does not destroy superconductivity, which coexists with high-temperature ferromagnetism [28−35]. The interplay between ferromagnetism and superconductivity offers rich physics. We observe pronounced in-gap edge states in $EuRbFe_4As_4$ at various step configurations and temperatures. Systematic STS measurements show these edge states are independent of bulk magnetism.

The 1144-type structure of $EuRbFe_4As_4$ comprises alternating $EuFe_2As_2$ and $RbFe_2As_2$ layers [Fig. 1(a), lattice constants $a = b \approx 0.38$ nm, $c \approx 1.34$ nm]. The Eu^{2+} layers order helically with a 90° rotation between adjacent layers [33]. This compound demonstrates both high-temperature superconductivity and magnetic order. We synthesize single crystals of $EuRbFe_4As_4$ using the RbAs-flux method. At zero field, $T_c \approx 36$ K, which decreases with applied magnetic field [Fig. 1(b)]. Magnetization measurements reveal diamagnetism below ~36 K and an antiferromagnetic cusp at T_m ~15 K [Fig. 1(c)].

Because Fe–As bonds are covalent, cleavage occurs along the van der Waals-bonded Eu or Rb layers. Each cleavage plane adsorbs half of the Eu or Rb atoms to maintain charge balance [29,31]. To minimize surface inhomogeneity, we cleave *in situ* at liquid-nitrogen temperature. Figure 1(d) shows a large flat terrace with Eu or Rb clusters and vacancy defects. dI/dV spectroscopy over 400 nm reveals a uniform superconducting gap irrespective of surface termination [Fig. 1(e)]. Cleavage surfaces exhibit one-unit-cell (1.34 nm) and half-unit-cell (0.67 nm) steps [Fig. 1(f) and Fig. S1 in the Supplementary Materials (SM)].

Figure 2(a) shows voltage-dependent dI/dV maps on a one-unit-cell step. At energies within the superconducting gap, we observe prominent electronic states on the step edge, absent outside the gap. These states show edge-state characteristics with intensity decaying exponentially into the terrace, with a decay length of ~1.8 nm [Fig. 2(b)]. This decay length remains consistent across different step types and tip-sample distances (see Fig. S3 in the SM). dI/dV spectra on and off the step edge show gap filling by a near-zero-energy peak at the step edge [Fig. 2(c)]. Unlike conventional superconductors, which typically feature a U-shaped energy gap, $EuRbFe_4As_4$ has a V-shaped gap that do not touches zero. This means that even within the gap, there are still some intrinsic states present. Because of these extra states, the edge of the material does not show the expected zero-energy peak. Therefore, we plotted the difference between the edge and the terrace STS spectra in insets of Figs. 2(c) and 2(f), allowing us to subtract out the background states and reveal the true nature of the edge behavior. Together, these data confirm in-gap edge states in $EuRbFe_4As_4$.

Received 30 July 2026; accepted 8 September 2026; published 1 October 2026
© 2026 Chinese Physical Society and IOP Publishing Ltd. All rights, including for text and data mining, AI training, and similar technologies, are reserved.

Check for updates

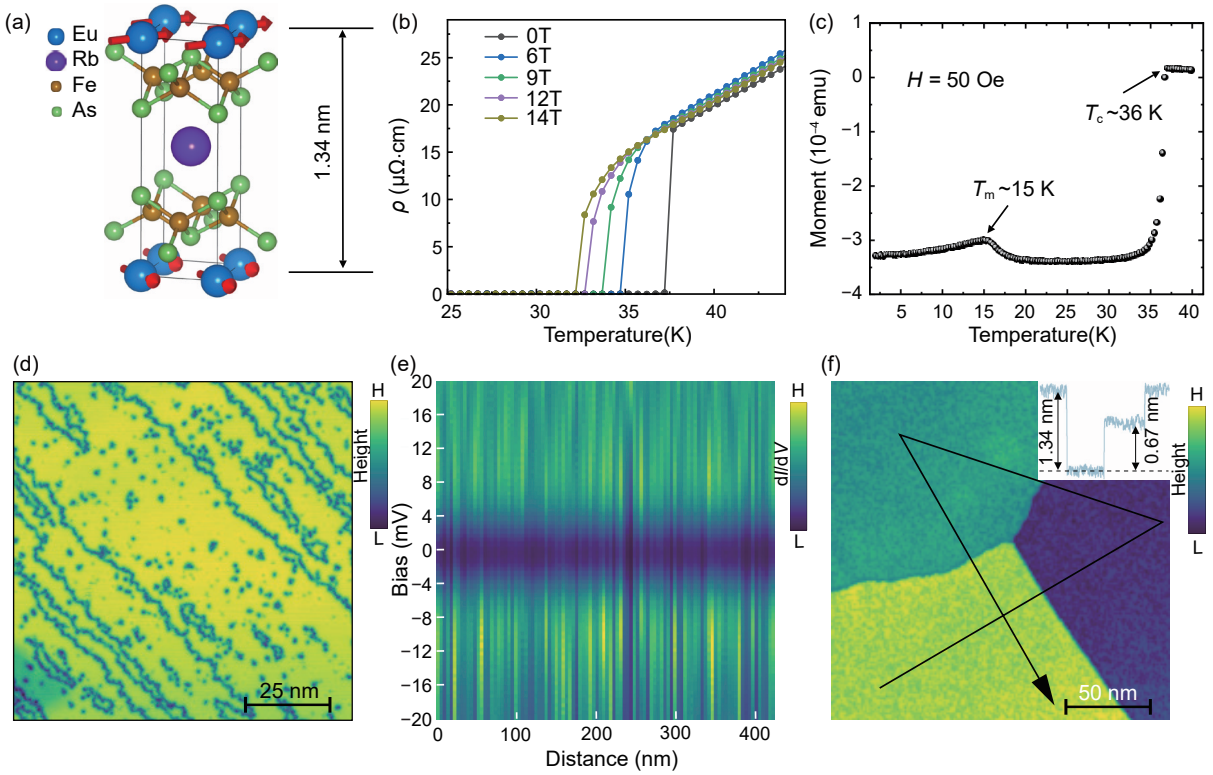

Fig. 1. Characterization of the iron pnictide superconductor $EuRbFe_4As_4$. (a) Crystal structure of one $EuRbFe_4As_4$ unit cell with the magnetic structure superimposed. The magnetic moments (red arrows) in neighboring Eu layers are oriented at 90° to each other. (b) Temperature-dependent resistance curves, demonstrating superconducting transitions under increasing magnetic fields. (c) Temperature dependence of magnetic moment for cooling in an external field of 50 Oe applied in the *ab* plane. (d) STM image (−1 V, 500 pA, 100 nm×100 nm) of $EuRbFe_4As_4$ surface showing random dotted and striped vacancies. (e) Diagram of position-dependent d*I*/d*V* spectra (−50 mV, 500 pA, V_{mod} = 1 mV) obtained over 400 nm scales revealing spatial uniform superconducting gaps. (f) An STM image (−1 V, 200 pA) on a $EuRbFe_4As_4$ showing a one-unit-cell step (1.34 nm) together with two half-unit-cell steps (0.67 nm). Inset: height variation along the black line in (f).

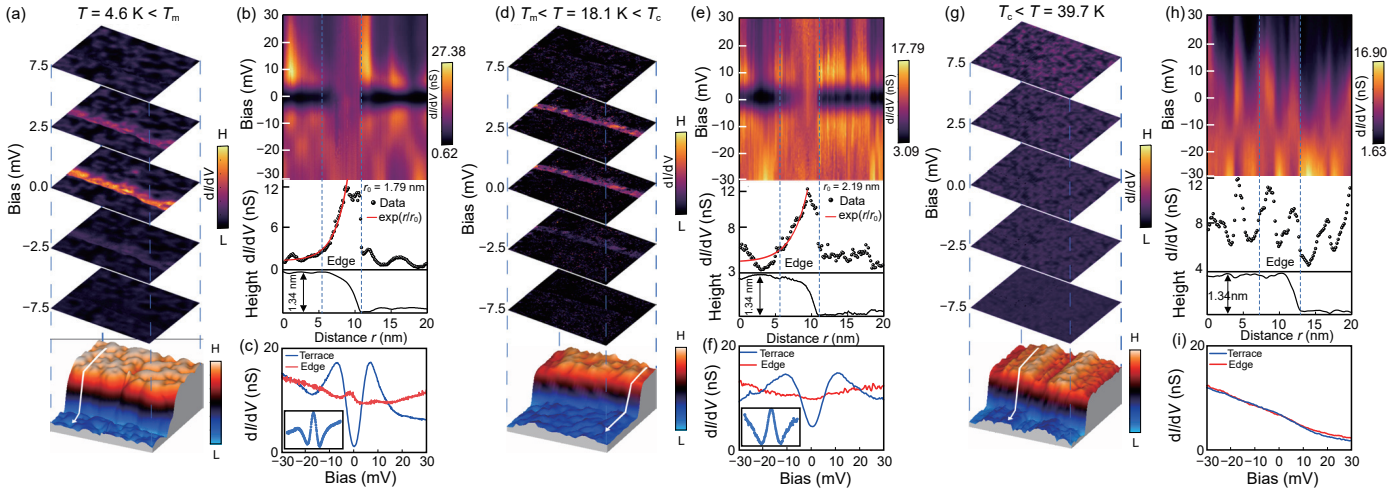

Fig. 2. Temperature dependence of in-gap edge states. (a), (d), (g) Various layers of a d*I*/d*V* grid (set point: −30 mV, 500 pA) at the indicated voltages in/near the superconducting gap together with their topographic images (−30 mV, 500 pA) (in 3D representation) at T = 4.6 K (a), T = 18.1 K (d), and T = 39.7 K (g), respectively. (b), (e), (h) Top panels: Diagram of position-dependent d*I*/d*V* spectra along the white line in (a), (d), (g), respectively. Center panels: The intensity distributions of d*I*/d*V* taken at 0 mV along the white lines in (a), (d), (g), respectively. The red curves show the exponential fittings of the decay of the states away from the edges. Bottom panels: Height profilers along the white lines in (a), (d), (g) showing a one-unit-cell step (1.34 nm). (c), (f), (i) Comparison of d*I*/d*V* spectra (−30 mV, 500 pA) on the terrace (blue line) and at the step edge (red line). The insets illustrate the difference in the differential conductance spectra between the edge and the terrace.

To probe the origin of these edge states, we perform systematic temperature-dependent experiments. Because the superconducting gap varies with tip-sample distance (see Fig. S2 in the SM), all measurements use identical conditions (−30 mV, 500 pA, V_{mod} = 0.3 mV), giving a gap of ~7 meV. At 18.1 K, which is above the magnetic transition (T_m) but below T_c, magnetism vanishes while superconductivity persists. The edge states persist [see Figs. 2(d) and 2(e)], ruling out magnetic domain boundaries in the Eu^{2+} layer as the sole origin.

Above T_c (39.7 K), the edge states vanish [Figs. 2(g) and 2(h)]. A comparison of the superconducting spectrum between the terrace and the step edge [Figs. 2(c), 2(f), and 2(i)] demonstrates that the presence or absence of magnetism does not affect the edge-state intensity

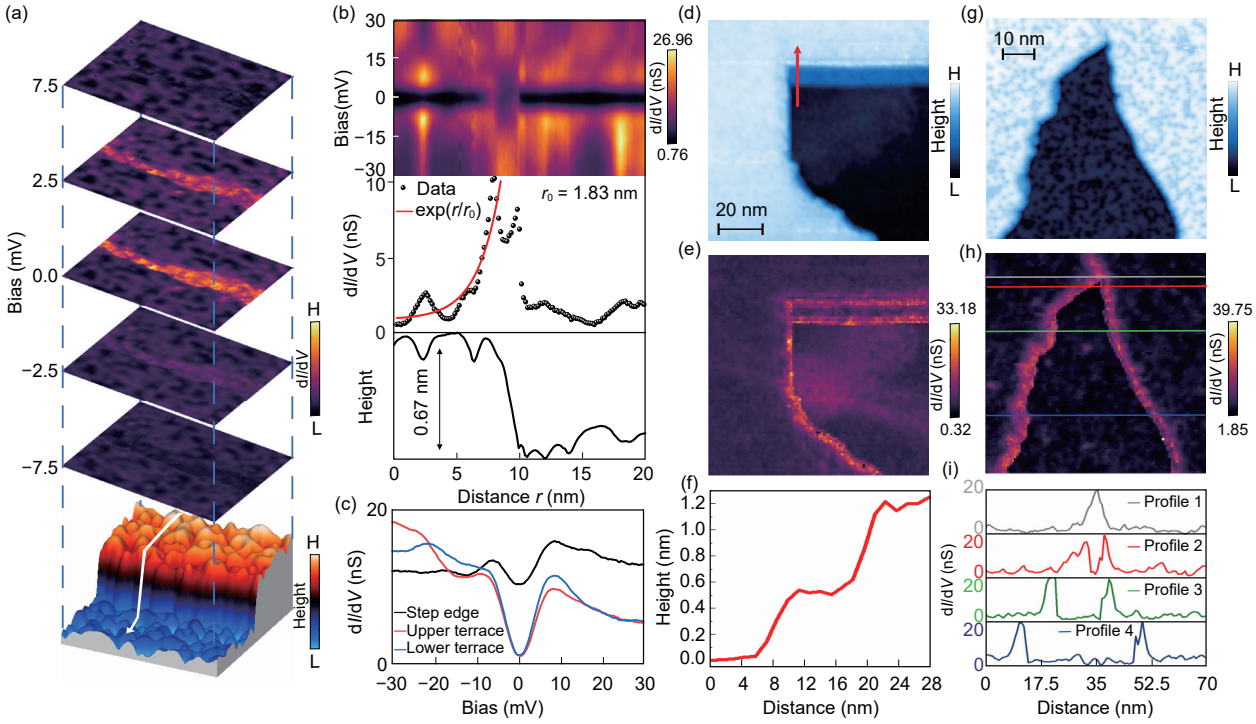

Fig. 3. In-gap edge states on various step configurations. (a) Various layers of a dI/dV grid (set point: −30 mV, 500 pA) at the indicated voltages in/near the superconducting energy gap taken on the area with a half-unit-cell step at $T = 4.6$ K. (b) Top panel: Diagram of position-dependent dI/dV spectra along the white line in (a). Center panel: The intensity distribution of dI/dV taken at 0 mV along the white line in (a). The red curve shows the exponential fitting of the decay of the state away from the edge. Bottom panel: Height variation along the white line in a showing a half-unit-cell step (0.67 nm). (c) Comparison of dI/dV spectra at the lower terrace (blue line), the step edge (black line), and the upper terrace (red line). (d) STM image (−20 mV, 500 pA) of a right angle formed by two half-unit-cell steps perpendicular to a one-unit-cell step. (e) dI/dV map at 0 mV on the same area as the image in (d). (f) Height variation along the red line in (d) showing two half-unit-cell steps. (g) STM image (−500 mV, 300 pA) of a sharp angle formed by two adjacent one-unit-cell steps. (h) dI/dV map (−20 mV, 500 pA) on the same area as the image in (g) at 0 mV. (i) The intensity distribution of dI/dV along the lines in (h).

when the sample remains superconducting. Upon exiting the superconducting state, the edge states disappear. These observations link edge-state formation to superconducting pairing rather than ferromagnetism.

To further characterize these edge states, we measure them on various step configurations. Half-unit-cell steps also host edge states with a decay length of ~1.8 nm [Figs. 3(a) and 3(b)]. Figure 3(c) compares dI/dV spectra on the upper (Rb-terminated) and lower (Eu-terminated) terraces and at the step edge, showing no significant difference in superconducting properties between terminations. This confirms that ferromagnetism does not affect superconductivity. We also image a right-angled step comprising two half-unit-cell steps and a one-unit-cell step [Figs. 3(d) and 3(e)]. Edge states appear on all steps, with no significant intensity difference between magnetic (Eu-terminated) and nonmagnetic (Rb-terminated) layers [Fig. 3(e)], confirming that these edge states are unrelated to ferromagnetism.

In two-dimensional topological insulators, helical edge states annihilate when two edges approach each other [5,36]. Figure 3(g) shows a wedge-shaped step with corresponding dI/dV map [Fig. 3(h)]. Edge-state intensities show no variation across differently oriented edges [Fig. 3(i)]. As the edges converge, their edge states do not couple [Fig. 3(h)]. This indicates chiral rather than helical edge states.

Although the exact origin of these edge states remains unclear, we note that the Fermi surfaces of $EuRbFe_4As_4$ revealed by ARPES measurements [37] resemble those of $CaKFe_4As_4$, exhibiting three hole-like pockets at the Γ point and two electron-like pockets at the corners of the Brillouin zone. Time reversal symmetry breaking and phase transitions at the domain wall were employed to interpret the in-gap states at the step edge of $CaKFe_4As_4$. A similar mechanism may also apply to our material. Besides this, there are other possible explanations. Short-range ferromagnetic fluctuations may also exist in our sample even at temperatures above T_m, which could break time-reversal symmetry and induce edge states.

In summary, we experimentally detected robust edge state signals at both one-unit-cell steps and half-unit-cell steps, as well as steps on different element terminated cleavage planes. Furthermore, our experiments revealed that these edge states do not originate from the material's intrinsic ferromagnetism or topological defects induced by lattice symmetry breaking but are closely related to superconducting pairing. Our findings here lay the groundwork for future theoretical studies.

Experimental Methods

Sample Preparation

Single crystals of $EuRbFe_4As_4$ are synthesized using the RbAs-flux method similar to that described in Ref. [38]. In order to get a clean and flat surface as well as avoiding a possible reconstruction of the surface for the cleaved sample, we cleaved $EuRbFe_4As_4$ single crystals in ultrahigh vacuum (UHV) at low temperature by circulating liquid nitrogen through the cooling stage where the material was placed. Then, we promptly transfer the cleaved sample *in situ* to the STM low-temperature scanning head.

STM Experiments

The experiments were conducted under an ultrahigh vacuum with a base pressure below 2×10^{-10} mbar. All STM experiments, except for the variable temperature experiments, were conducted at 4.6 K. The STM tips were prepared from polycrystalline tungsten wires by electrochemical etching and calibrated on a clean Au(111) surface before all STM measurements. Differential conductance (local density of states) measurements were performed using the standard lock-in technique with 971 Hz frequency and bias modulation as also detailed in the figure captions.

Author Contributions

The manuscript was written through contributions of all authors. All authors have given approval to the final version of the manuscript.

Acknowledgments

This work was supported by the National Natural Science Foundation of China (NSFC) (Grant Nos. 92365302, 12488101, 12474156, 22325203, 52102336, 12474121, 12274283, 12374148, and 12334008), the Ministry of Science and Technology of China (Grant Nos. 2020YFA0309000, 2024YFA1410100, 2025YFE0201200, 2022YFA1402702, and 2021YFA1401600), the Science and Technology Commission of Shanghai Municipality (Grant Nos. 2019SHZDZX01, 20QA1405100, and 24LZ1401000), the Cultivation Project of Shanghai Research Center for Quantum Sciences (Grant No. LZPY2024-04), and the innovation program for Quantum Science and Technology (Grant No. 2021ZD0302500).

References

[1] Kane C L and Mele E J 2005 *Phys. Rev. Lett.* **95** 226801
[2] Bernevig B A, Hughes T L, and Zhang S C 2006 *Science* **314** 1757
[3] Yang F, Miao L, Wang Z F, Yao M Y, Zhu F, Song Y R, Wang M X, Xu J P, Fedorov A V, Sun Z, Zhang G B, Liu C, Liu F, Qian D, Gao C L, and Jia J F 2012 *Phys. Rev. Lett.* **109** 016801
[4] Drozdov I K, Alexandradinata A, Jeon S, Nadj-Perge S, Ji H, Cava R J, Andrei Bernevig B, and Yazdani A 2014 *Nat. Phys.* **10** 664
[5] Sessi P, Di Sante D, Szczerbakow A, Glott F, Wilfert S, Schmidt H, Bathon T, Dziawa P, Greiter M, Neupert T, Sangiovanni G, Story T, Thomale R, and Bode M 2016 *Science* **354** 1269
[6] Reis F, Li G, Dudy L, Bauernfeind M, Glass S, Hanke W, Thomale R, Schäfer J, and Claessen R 2017 *Science* **357** 287
[7] Peng L, Yuan Y, Li G, Yang X, Xian J J, Yi C J, Shi Y G, and Fu Y S 2017 *Nat. Commun.* **8** 659
[8] Yin J X, Ma W, Cochran T A *et al*. 2020 *Nature* **583** 533
[9] Lüpke F, Waters D, De La Barrera S C, Widom M, Mandrus D G, Yan J, Feenstra R M, and Hunt B M 2020 *Nat. Phys.* **16** 526
[10] Nie X A, Li S, Yang M, Zhu Z, Xu H K, Yang X, Zheng F, Guan D, Wang S, Li Y Y, Liu C, Li J, Zhang P, Shi Y, Zheng H, and Jia J 2020 *ACS Nano* **14** 2366
[11] Xu H K, Gu M, Fei F, Gu Y S, Liu D, Yu Q Y, Xue S S, Ning X H, Chen B, Xie H, Zhu Z, Guan D, Wang S, Li Y, Liu C, Liu Q, Song F, Zheng H, and Jia J 2022 *ACS Nano* **16** 9810
[12] Zhao C, Li L, Zhang L, Qin J, Chen H, Xia B, Yang B, Zheng H, Wang S, Liu C, Li Y, Guan D, Cui P, Zhang Z, and Jia J 2022 *Phys. Rev. Lett.* **128** 206802
[13] Ivanov D A 2001 *Phys. Rev. Lett.* **86** 268
[14] Fu L and Kane C L 2008 *Phys. Rev. Lett.* **100** 096407
[15] Wang M X, Liu C, Xu J P, Yang F, Miao L, Yao M Y, Gao C L, Shen C, Ma X, Chen X, Xu, Z A, Liu Y, Zhang S C, Qian D, Jia J F, and Xue Q K 2012 *Science* **336** 52
[16] Sun H H, Zhang K W, Hu L H, Li C, Wang G Y, Ma H Y, Xu Z A, Gao C L, Guan D D, Li Y Y, Liu C, Qian D, Zhou Y, Fu L, Li S C, Zhang F C, and Jia J F 2016 *Phys. Rev. Lett.* **116** 257003
[17] Wang D, Kong L, Fan P, Chen H, Zhu S, Liu W, Cao L, Sun Y, Du S, Schneeloch J, Zhong R, Gu G, Fu L, Ding H, and Gao H J 2018 *Science* **362** 333
[18] Liu Q, Chen C, Zhang T, Peng R, Yan Y J, Wen C H P, Lou X, Huang Y L, Tian J P, Dong X L, Wang G W, Bao W C, Wang Q H, Yin Z P, Zhao Z X, and Feng D L 2018 *Phys. Rev. X* **8** 041056
[19] Kong L, Zhu S, Papaj M, Chen H, Cao L, Isobe H, Xing Y, Liu W, Wang D, Fan P, Sun Y, Du S, Schneeloch J, Zhong R, Gu G, Fu L, Gao H J, and Ding H 2019 *Nat. Phys.* **15** 1181
[20] Machida T, Sun Y, Pyon S, Takeda S, Kohsaka Y, Hanaguri T, Sasagawa T, and Tamegai T 2019 *Nat. Mater.* **18** 811
[21] Chen C, Jiang K, Zhang Y, Liu C, Liu Y, Wang Z, and Wang J 2020 *Nat. Phys.* **16** 536
[22] Nadj-Perge S, Drozdov I K, Li J, Chen H, Jeon S, Seo J, MacDonald A H, Bernevig B A, and Yazdani A 2014 *Science* **346** 602
[23] Wang Z F, Zhang H, Liu D, Liu C, Tang C, Song C, Zhong Y, Peng J, Li F, Nie C, Wang L, Zhou X J, Ma X, Xue Q K, and Liu F 2016 *Nat. Mater.* **15** 968
[24] Yuan Y, Li W, Liu B, Deng P, Xu Z, Chen X, Song C, Wang L, He K, Xu G, Ma X, and Xue Q K 2018 *Nano Lett.* **18** 7176
[25] Wang Z Y, Rodriguez J O, Jiao L, Howard S, Graham M, Gu G D, Hughes T L, Morr D K, and Madhavan V 2020 *Science* **367** 104
[26] Liu S, Nie S M, Qi Y P, Guo Y F, Yuan H T, Yang L X, Chen Y L, Wang M X, and Liu Z K 2021 *Chin. Phys. Lett.* **38** 077302
[27] Cao L, Li G, Liu W, Liu Y B, Chen H, Xing Y, Kong L, Yang F, Hu Q, Li M, Zhou X, Chen Z, Ke C, Hu L, Cao G H, Wu C, Ding H, and Gao H J 2024 *Chin. Phys. Lett.* **41** 117401
[28] Mebratie G, Negussie T, and Kahsay G 2025 *Nano Sel.* **6** e202400124
[29] Zhao H, Blackwell R, Thinel M, Handa T, Ishida S, Zhu X, Iyo A, Eisaki H, Pasupathy A N, and Fujita K 2023 *Nature* **618** 940
[30] Hemmida M, Winterhalter-Stocker N, Ehlers D, von Nidda H A K, Yao M, Bannies J, Rienks E D L, Kurleto R, Felser C, Büchner B, Fink J, Gorol S, Förster T, Arsenijevic S, Fritsch V, and Gegenwart P 2021 *Phys. Rev. B* **103** 195112
[31] Stolyarov V S, Pervakov K S, Astrakhantseva A S, Golovchanskiy I A, Vyalikh D V, Kim T K, Eremeev S V, Vlasenko V A, Pudalov V M, Golubov A A, Chulkov E V, and Roditchev D J 2020 *Phys. Chem. Lett.* **11** 9393
[32] Vlasenko V, Pervakov K, and Gavrilkin S 2020 *Supercond. Sci. Technol.* **33** 084009
[33] Iida K, Nagai Y, Ishida S, Ishikado M, Murai N, Christianson A D, Yoshida H, Inamura Y, Nakamura H, Nakao A, Munakata K, Kagerbauer D, Eisterer M, Kawashima K, Yoshida Y, Eisaki H, and Iyo A 2019 *Phys. Rev. B* **100** 014506
[34] Stolyarov V S, Casano A, Belyanchikov M A, Astrakhantseva A S, Grebenchuk S Yu, Baranov D S, Golovchanskiy I A, Voloshenko I, Zhukova E S, Gorshunov B P, Muratov A V, Dremov V V, Vinnikov L Ya, Roditchev D, Liu Y, Cao G H, Dressel M, and Uykur E 2018 *Phys. Rev. B* **98** 140506
[35] Kawashima K, Kinjo T, Nishio T, Ishida S, Fujihisa H, Gotoh Y, Kihou K, Eisaki H, Yoshida Y, and Iyo A 2016 *J. Phys. Soc. Jpn.* **85** 064710
[36] Yu S, Deng J, Liu W, Zhang Y, Sun Y, Dhale N, Li S, Ma W, Wang Z, Wu P, Liang Z, Zhang X, Lv B, Wang Z, Wang Z, and Chen X 2024 *Phys. Rev. X* **14** 041048
[37] Kim T K, Pervakov K S, Evtushinsky D V, Jung S W, Poelchen G, Kummer K, Vlasenko V A, Sadakov A V, Usoltsev A S, Pudalov V M, Roditchev D, Stolyarov V S, Vyalikh D V, Borisov V, Valentí R, Ernst A, Eremeev S V, and Chulkov E V 2021 *Phys. Rev. B* **103** 174517
[38] Bao J K, Willa K, Smylie M P *et al*. 2018 *Cryst. Growth Des.* **18** 3517